

Rydberg blockade with multivalent atoms: engineering van der Waals interactions

Turker Topcu^{1,2} and Andrei Derevianko¹

¹*Department of Physics, University of Nevada, Reno, Nevada 89557, USA*

²*Department of Mathematics, Virginia Tech, Blacksburg, Virginia 24061, USA*

(Dated: September 20, 2022)

We investigate the effect of series perturbation on the second order dipole-dipole interactions between strontium atoms in the $5sns(^1S_0)$ and $5snp(^1P_1)$ Rydberg states as a means of engineering long-range interactions between atoms. The series perturbation in these atoms enables modifying the strength and the sign of the interaction by varying the principal quantum number n of the Rydberg electron. We utilize experimentally available data to estimate the importance of perturber states, and find that van der Waals interaction between two strontium atoms in the $5snp(^1P_1)$ states shows strong peaks outside the anticipated hydrogenic n^{11} scaling. We identify this to be the result of the perturbation of $5snd(^1D_2)$ intermediate states by the $4d^2(^1D_2)$ and $4dn's(^1D_2)$ states in the $n < 20$ range. This demonstrates that divalent atoms offer a unique advantage for generating substantially stronger or weaker inter-atomic interactions than those that can be achieved using alkali metal atoms. This is due to the highly perturbed spectra of divalent atoms and other multivalent atoms that can persist up to high n . Such irregularities can be especially useful in engineering asymmetric Ry blockade requiring simultaneous presence of both “weak” and “strong” interactions.

PACS numbers: 32.80.Ee, 34.20.Cf, 37.10.Jk

I. INTRODUCTION

Long-range interactions between Rydberg (Ry) atoms are a useful resource in realizing conditional quantum dynamics, enabling a number of applications in quantum information processing (QIP) with neutral atoms [1–4]. Mediated by strong interactions between Ry atoms, the Rydberg blockade mechanism, which prohibits simultaneous excitation of two nearby Ry atoms, has particularly expanded the QIP toolbox. Applications of the Rydberg blockade include quantum logic gates [4, 5], simulation of exotic quantum many-body systems [6, 7], study of strongly-correlated systems [8, 9], and multiparticle entanglement generation [10]. Strong Rydberg atom interactions have also facilitated the realization of strongly interacting individual photons paving the way for quantum non-linear optics at the single photon level [11, 12].

Most of practical applications of Rydberg blockade have so far focused on alkali-metal atoms, *i.e.* atoms with a single valence electron outside a closed-shell core. Moving to multivalent atoms offers new possibilities in engineering quantum systems [13]. Divalent atoms, such as group-II atoms (*e.g.*, Mg, Ca, Sr) and group-II-like atoms such as Yb, Hg, Cd, and Zn are the simplest examples of *multivalent* atoms. While in this paper we focus on divalent atoms, our qualitative observations remain valid for more complicated multivalent atoms, such as holmium [14] and erbium [15]. Divalent atoms possess the advantage of an extra valence electron, which provides easier trapping in tight optical lattices [16, 17]. This is greatly beneficial as the optical trapping is essential for neutral-atoms QIP experiments due to the long coherence times that can be achieved. Coupled with mature experimental techniques for cooling and trapping divalent atoms [18–21], divalent atoms can offer additional advantages in QIP schemes compared to alkalis.

Recently, high-fidelity trapping and single-qubit operations in arrays of ^{171}Yb were reported [22, 23] offering robust spin-qubits due to its 1/2 nuclear spin.

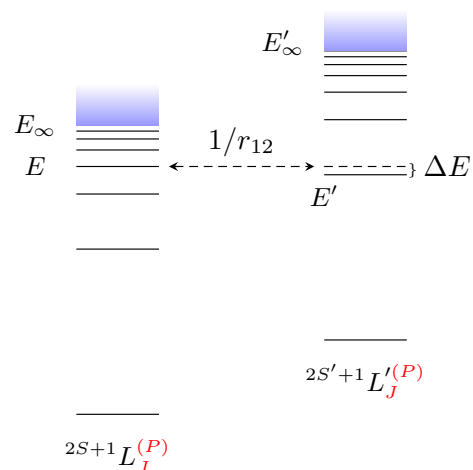


FIG. 1: (Color online) Illustration of series interaction where two Rydberg series $2S+1 L_J^{(P)}$ and $2S'+1 L'_J^{(P)}$ with the same total J and parity P converge to different ionization thresholds E_∞ and E'_∞ . If two states from these series happen to be close in energy (states labeled E and E'), the Coulomb interaction $1/r_{12}$ can mix these states. The mixing is most prominent when the energy difference ΔE is small compared to the Coulomb interaction matrix element.

The leading long-range interaction between Ry atoms in the same parity states is the second-order dipole-dipole (or the van der Waals) interaction. The van der Waals (vdW) interaction between alkali-metal atoms scales as n^{11} , n being the principal quantum number of Ry electron. Here we point out a significant deviation from this scaling law for multivalent atoms. This feature is unique

for multivalent atoms as it is caused by the so-called Ry series interaction. Indeed, highly-excited energy levels of divalent atoms can be characterized by the electronic configuration $n\ell n_r \ell_r$, where n_r and ℓ_r are principal and orbital quantum numbers of the Rydberg electron while, n, ℓ are those for the “spectator” electron. Consider two Ry series $n_1 \ell_1 n_r \ell_r$ and $n_2 \ell_2 n'_r \ell'_r$ ($n_1 \ell_1$ and $n_2 \ell_2$ are fixed, while n_r and n'_r are scanned through the series for given ℓ_r and ℓ'_r). Generically, such series exhibit the usual hydrogen-like behavior of energy levels. However, at some values of n_r and n'_r , the two series may come close to being degenerate (see Fig. 1). For such cases, if the symmetries (the total angular momenta and parities) of the two series are identical, neither of the states remains a “good” eigenstate of the atomic Hamiltonian and the levels are mixed by the off-diagonal Coulomb interaction between the configurations. This mechanism is well-known in spectroscopy [24] and is referred to as the series interaction or series perturbation.

As we demonstrate below, the series interaction leads to substantial deviations from the n^{11} scaling law, with Ry states of the same series exhibiting both relatively small and large van der Waals interactions. The vdW interaction, which depends on the interatomic separation R as R^{-6} , arises in the second-order in the dipole-dipole interaction between two Ry atoms. As any second-order contribution, it is expressed as a sum over intermediate states with the energy denominator. The energy difference between the reference Ry+Ry states and an intermediate diatom state, entering the denominator, can deviate from the nominal behavior due to the series interaction of the intermediate state with another series of the same symmetry. Namely, this mechanism of intermediate state series perturbation is the cause of the irregularities in the van der Waals interaction strength. Such irregularities can be especially useful in asymmetric Ry blockade [13] which requires simultaneous presence of both “weak” and “strong” interactions.

Having in mind an eventual application of Rydberg blockade in Heisenberg-limited metrology, as a specific example, we focus on Sr for its common use in optical lattice clocks [25]. We evaluate the relevant C_6 coefficients for vdW interactions between a pair of Sr atoms in the $5sns(^1S_0)$ and $5snp(^1P_1)$ states. We show that the vdW interaction between two Sr atoms in the $5snp(^1P_1)$ states display highly non-monotonic behavior for low- n states ($n \lesssim 20$), strongly deviating from the alkali-like smooth n^{11} scaling of the vdW interaction strength. We trace the origin of this behavior to unusually small energy denominators in the second-order energy expression resulting from the strong variation in atomic energies due to the series interaction. In particular, the $nP+nP \rightarrow nD+(n-1)D$ channel contributes to the C_6 coefficients with small energy denominators due to the highly perturbed nature of the $5snd(^1D_2^e)$ series in Sr. Researching the literature, we find that the $5snd(^1D_2^e)$ series is perturbed by the $4d^2(^1D_2^e)$, $5p^2_{3/2}(^1D_2^e)$ and $4d6s(^1D_2^e)$ states, which lie below the ionization thresh-

old of the $5snd(^1D_2^e)$ series at 45,932 cm⁻¹ [26]. Particularly, the $4d6s(^1D_2^e)$ state perturbs states with $n = 11 - 17$, $5p^2(^1D_2^e)$ perturbs states with $n = 5 - 6$ and $4d^2(^1D_2^e)$ state perturbs the state with $n = 12$ in the $5snd(^1D_2^e)$ series. For the interaction between two Sr atoms in the $5sns(^1S_0^e)$ states, we do not see this non-monotonic behavior in the n -range we consider. Similar effects on dynamic polarizabilities in Rydberg electrons attached to a hyperfine-split core state have been predicted [14, 27] for some alkaline earth and lanthanide atoms for $n \geq 50$.

The paper is organized as follows: in Sec. II, we start with a brief description of the mechanism behind the series perturbation in divalent atoms. Then in Sec. III, we present our formalism and describe the computational framework. Results of our calculations for the $^1S_0 + ^1S_0$ and $^1P_1 + ^1P_1$ vdW interaction coefficients are presented in Sec. IV. Here we discuss the effects of the perturber states on the van der Waals interactions, which are pronounced for the $5snp(^1P_1)$ Rydberg states with $n \lesssim 20$. In Sec. V, we discuss the angular dependence of the vdW interactions. Finally, we draw conclusions in Sec. VI. Atomic units ($\hbar = m_e = |e| \equiv 1$) are used throughout unless stated otherwise.

II. SERIES PERTURBATION IN DIVALENT ATOMS

We start by presenting a more detailed account of the series interaction mechanism and describe how it also results in van der Waals interactions that can strongly deviate from the n^{11} alkali-metal-atom scaling law. Fig. 1 illustrates the basic qualitative picture. Two Rydberg series identified with the terms $^{2S+1}L_J^{(P)}$ and $^{2S+1}L_J^{(P)}$ have identical total angular momenta J and parities P . In the limit $n_r \rightarrow \infty$ these series converge to different thresholds labeled as E_∞ and E'_∞ . Two levels, E and E' , of these series are nearly degenerate in energy, which can be quantified by comparing their energy separation ΔE to the off-diagonal matrix element of the Coulomb interaction evaluated between these nearly-degenerate states. Because of the accidental near degeneracy, the two levels repel each other, as long the Coulomb matrix elements do not vanish. The two series must have the same J and P , otherwise the Coulomb matrix element would vanish. Typically, the Rydberg states lying above the perturbing state are shifted up in energy whereas the states below the perturbing state are shifted down [24].

The effect of series perturbation is more pronounced for states of higher angular momenta. The underlying reason for such an enhancement is that the Rydberg electron is less influenced by the singly ionized core in higher angular momentum states, such as the $5sn\ell$ states of Sr and these states are more hydrogenic in character. This increases the possibility of running into perturber states with close lying energies because the energies of the higher ℓ -states start to become independent of ℓ for

a given n as in hydrogenic systems. This increases the density of states, thereby increasing the number of states that are likely to be perturbed by a single perturber. For example, although the $5sns(^1S_0)$ series of Sr is essentially unperturbed above $n = 10$, the $5snd(^1D_2)$ series is substantially perturbed [26].

For two identical atoms separated by a distance R and in fixed magnetic sublevels, the vdW interaction reads

$$\delta E_{\text{vdW}}(R) = \sum_{j,k} \frac{|\langle \psi(\text{I}) | \langle \psi(\text{II}) | V_{DD}(R) | \phi_j(\text{I}) \rangle | \phi_k(\text{II}) \rangle|^2}{2E_\psi - (E_j + E_k)}. \quad (1)$$

Here I and II label the two atoms. In our case, the electronic states of the two atoms, $\psi(\text{I})$ and $\psi(\text{II})$, are the same, and are either $|5sns(^1S_0)\rangle$ or $|5snp(^1P_1)\rangle$. The intermediate states $|\phi\rangle$ run through the $|5sn'p(^1P_1)\rangle$ states for the $|5sns(^1S_0)\rangle$ target states, and they run over $|5sn's(^1S_0)\rangle$, $|5sn'd(^1D_2)\rangle$ and $(|5sn's(^1S_0)\rangle + |5sn'd(^1D_2)\rangle)/\sqrt{2}$ for the $|5snp(^1P_1)\rangle$ states (here we assumed that the total spin is a good quantum number). The dipole-dipole interaction between two atoms (I and II) can be decomposed as

$$V_{DD}(R) = -\frac{1}{R^3} \sum_{\mu} w_{\mu}^{(1)} D_{\mu}^{(1)}(\text{I}) D_{-\mu}^{(1)}(\text{II}), \quad (2)$$

where $w_{\mu}^{(1)} = 1 + \delta_{\mu,0}$, and the conventional electric-dipole operators are defined through their spherical-basis components as

$$D_{\mu}^{(1)} = -\sum_k r_k C_{\mu}^{(1)}(\hat{\mathbf{r}}_k). \quad (3)$$

Here $C_{\mu}^{(L)}(\hat{\mathbf{r}}) = \sqrt{4\pi/(2L+1)} Y_{\mu}^{(L)}(\hat{\mathbf{r}})$ are the normalized spherical harmonics and k runs over atomic electrons. In Eq. (2), the quantization axis is directed along the internuclear axis. Clearly, the vdW interaction (1) exhibits the $\propto R^{-6}$ scaling:

$$\delta E_{\text{vdW}}(R) = \frac{1}{R^6} \sum_{j,k} \frac{|V_{j,k}|^2}{\Delta E_{j,k}} = -\frac{C_6}{R^6}. \quad (4)$$

Here we replaced the numerator in (1) with $|V_{j,k}|^2/R^6$, and the denominator with $\Delta E_{j,k}$.

The expression (1) sensitively depends on energy denominators, thereby accidental near-degeneracies between the target and intermediate states can result in strong deviations from the n^{11} hydrogenic scaling behavior of the long-range interaction strengths. As discussed below, we observe such an effect in the van der Waals interactions between two $5snp(^1P_1)$ Sr Rydberg atoms, as this interaction has an intermediate excitation channel $5snp(^1P_1) + 5snp(^1P_1) \rightarrow 5sn'd(^1D_2) + 5sn'd(^1D_2)$ and the $5snd(^1D_2)$ states are strongly perturbed below $n \simeq 20$.

In our calculations, we assume that the LS-coupling scheme holds in the Ry series. This is not necessarily true for all n -ranges in Sr, particularly in Ry series

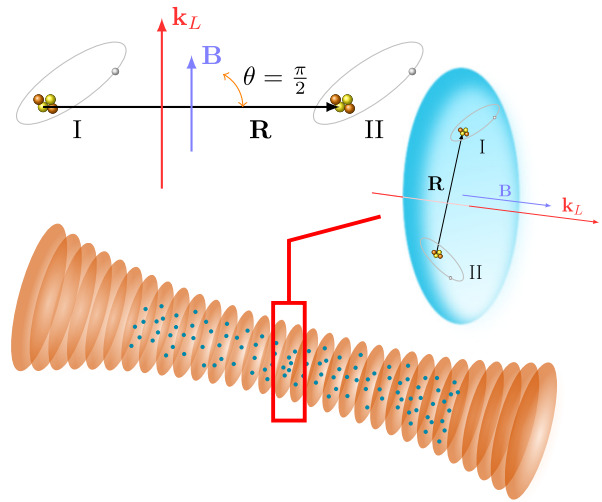


FIG. 2: (Color online) One-dimensional lattice geometry described in the text in which atoms are trapped in pancake shaped clouds at each lattice site. Application of a magnetic field \mathbf{B} perpendicular to the plane of the pancake clouds lifts the Zeeman degeneracy where the quantization axis is perpendicular to the internuclear axis $\hat{\mathbf{R}}$ between atoms in each cloud. Here \mathbf{k}_L is the wave vector of the lasers making up the optical lattice.

with high angular momentum L . For example, in the $5snd(D_2)$ Ry states, the series with the singlet and the triplet characters significantly mix for $n = 15$ and 16 , whereas the mixing is negligible for all other n up to 30 [26]. In the case of the $5s15d(D_2)$ states, roughly 35% of the channel is of the $5s15d(^1D_2)$ character, and 55% is of the $5s15d(^3D_2)$ character. Other series of interest with lower angular momenta, *i.e.* $5sns(S_0)$ and $5snp(P_1)$, do not display this mixing in the n -ranges we are interested in this work. The mixing between the $5snd(^1D_2)$ and $5snd(^3D_2)$ series, although appreciable for $n = 15$ and 16 , does not affect our qualitative conclusions, due to the fact that the dipole matrix elements connecting 1P_1 and 3D_2 states are suppressed by a factor of $\propto \alpha^2 \sim 10^{-4}$ as this transition is nonrelativistically forbidden.

To highlight the effect of series perturbation in the most clear fashion, we evaluate the vdW coefficients C_6 for a non-degenerate manifold of magnetic substates. Zeeman degeneracy can be lifted by an application of external B-field and working with atoms trapped in a pancake-shaped cloud, so that the interactions occur in the pancake plane (internuclear axes for all diatoms lie in that plane). Fig. 2 shows this trapping geometry. It is ubiquitous in practical realizations of optical lattice clocks [28–30]. An external magnetic field \mathbf{B} can be applied along the lattice axis, making the quantization axis orthogonal to \mathbf{R} , the internuclear separation. For a sufficiently strong magnetic field, we may neglect the vdW-induced mixing of magnetic sublevels and focus on a single M_B sublevel, with M_B being the projection of the atomic angular momentum along the B-field. The quan-

tization axis in Eq. (1) is along the internuclear axis $\hat{\mathbf{R}}$. We rotate the dipole interaction V_{DD} from $\hat{\mathbf{R}}$ to the direction of the B -field by rotating dipole operators $D_\mu^{(1)}$ in Eq. (2) by the angle θ with respect to the pancake plane. Such rotation can be achieved by the conventional sequence of rotations through the Euler angles $\alpha = 0$, $\beta = \theta$ and $\gamma = 0$. If we denote the rotation operator by \hat{S} , the normalized spherical harmonics in Eq. (3) transform as

$$C_{M_K}^{(K)}(\hat{S}\hat{\mathbf{r}}) = \sum_{M=-K}^K C_M^{(K)}(\hat{\mathbf{r}}) \mathbb{D}_{M,M_K}^{(K)}(0, \theta, 0), \quad (5)$$

where $\mathbb{D}_{M,M'}^{(K)}(\alpha, \theta, \gamma)$ are the Wigner D -functions [31]. This results in the rotated dipole operator

$$D_\mu^{(1)}(\hat{S}\hat{\mathbf{r}}) = - \sum_j r_j \sum_{M=-1}^1 C_M^{(1)}(\hat{\mathbf{r}}_j) \mathbb{D}_{M,\mu}^{(1)}(0, \theta, 0). \quad (6)$$

Notation M_x in the following text denotes the specific case of $\theta = \pi/2$ when the B -field points along the laser propagation axis. We perform our numerical calculations for this case and then extend the analysis to an arbitrary angle.

III. VAN DER WAALS INTERACTIONS

Now we focus on computing the vdW interaction between two identical Rydberg atoms. Because it is second order in the dipole-dipole interaction, vdW contribution to the long-range molecular potential varies as $1/R^6$ with the inter-atomic separation and corresponds to the $-C_6/R^6$ term in the conventional multipole expansion of the long-range interactions. We are interested in the interactions between two $5sns(^1S_0)$ or two $5snp(^1P_1)$ state atoms. When evaluating the interaction between the $5snp(^1P_{1,M_B})$ and $5snp(^1P_{1,M'_B})$ atoms, we will consider the stretched $M_B = M'_B = 1$ state. For two spherically-symmetric $5sns(^1S_0)$ atoms the rotation of quantization axis is irrelevant and $M_B = M'_B \equiv 0$.

Derivation of the vdW interaction expressions in the LS coupling is given in the Appendix. The vdW interaction for two Sr atoms in the $5sns(^1S_0)$ Rydberg states can be expressed as

$$C_6(5sns(^1S_0)(\text{I}) 5sns(^1S_0)(\text{II})) = - \frac{2}{3} \sum_{n_2, n'_2} \frac{|\langle ns || d || n_2p \rangle|^2 |\langle ns || d || n'_2p \rangle|^2}{2E_{ns} - (E_{n_2p} + E_{n'_2p})}, \quad (7)$$

which involves the reduced matrix elements of the atomic dipole moment operators. The n_2p and n'_2p single-electron states reflect the electronic configurations of the intermediate dimer states $|5sn_2p(^1P_1)\rangle_{\text{I}} |5sn'_2p(^1P_1)\rangle_{\text{II}}$. Because we work in the LS coupling scheme, the contributions from the 3P_1 intermediate states are ignored because they contribute through spin-changing transitions, which are forbidden in the non-relativistic formalism.

For the interaction between two $5snp(^1P_1)$ atoms in the $M_x = M'_x = 1$ magnetic substates,

$$C_6(5snp(^1P_{1,1_x})(\text{I}) 5snp(^1P_{1,1_x})(\text{II})) = \frac{1}{36} S_{ss} + \frac{181}{3600} S_{dd} + \frac{11}{72} S_{sd}. \quad (8)$$

The structure of this expression reflects two possible single-atom dipole excitation channels $5snp(^1P_1) \rightarrow 5sn_2s(^1S_0)$ and $5snp(^1P_1) \rightarrow 5sn_2d(^1D_2)$ with the reduced sums S defined as

$$S_{ss} = - \sum_{n_2, n'_2} \frac{|\langle np || d^{(1)} || n_2s \rangle|^2 |\langle np || d^{(1)} || n'_2s \rangle|^2}{2E_{np} - (E_{n_2s} + E_{n'_2s})},$$

$$S_{dd} = - \sum_{n_2, n'_2} \frac{|\langle np || d^{(1)} || n_2d \rangle|^2 |\langle np || d^{(1)} || n'_2d \rangle|^2}{2E_{np} - (E_{n_2d} + E_{n'_2d})},$$

$$S_{sd} = - \sum_{n_2, n'_2} \frac{|\langle np || d^{(1)} || n_2s \rangle|^2 |\langle np || d^{(1)} || n'_2d \rangle|^2}{2E_{np} - (E_{n_2s} + E_{n'_2d})}.$$

A. Uncertainty Estimates

The van der Waals interaction energy in Eq. (4) depends sensitively on the energy denominators, and experimental uncertainties in the measured energies can potentially affect our results. In our calculations of the C_6 coefficients from Eq. (4), we take the uncertainty of the measured energy level data into account when available, and report the error bars resulting from the propagation of the energy uncertainties:

$$(\delta C_6)^2 = \sum_{j,k} \left(\left| \frac{2V_{j,k}}{\Delta E_{j,k}} \right| \delta(V_{j,k}) \right)^2 + \left(\left| \frac{V_{j,k}^2}{\Delta E_{j,k}^2} \right| \delta(\Delta E_{j,k}) \right)^2, \quad (10)$$

$$\delta(\Delta E_{j,k}) = \sqrt{(2\delta(\Delta E_\psi))^2 + \delta(\Delta E_j)^2 + \delta(\Delta E_k)^2} \quad (11)$$

Here we add the uncertainties in quadrature assuming a normal distribution of measured values with standard deviations δE_ψ , δE_j , and δE_k . For example, when evaluating $\delta(\Delta E_{j,k})$ for the vdW interaction of two $5snp(^1P_1)$ states, $\delta(\Delta E_\psi)$ is the energy uncertainty $\delta(\Delta E_{5snp(^1P_1)})$, and the uncertainties δE_j and δE_k are one of $\delta E_{5sns(^1S_0)}$ and $\delta E_{5snd(^1D_2)}$. Furthermore, we calculate the matrix elements using a one-electron model potential described in the next section; we will demonstrate that uncertainties in matrix elements in Eq. (10), which can be viewed as errors made in the matrix elements by using a model potential, can be ignored near energy degeneracies. Thereby,

$$(\delta C_6)^2 \approx \sum_{j,k} \left(\left| \frac{V_{j,k}^2}{\Delta E_{j,k}^2} \right| \delta(\Delta E_{j,k}) \right)^2. \quad (12)$$

In our calculations, the energies of the $5sns(^1S_0)$, $5snp(^1P_1)$ and $5snd(^1D_2)$ states in the range $6 \leq n \leq 20$ come from Ref. [32], which are data listed in the online NIST database. The data reported in [32] include uncertainties, which we use to estimate the errors in our calculated C_6 coefficients in $6 \leq n \leq 20$. We use energies from [33] for $5sns(^1S_0)$ in the range $21 \leq n \leq 40$, and from [34] in $41 \leq n \leq 70$. These older data do not come with experimental uncertainties, which is why there are no error bars in Fig. 3 for states with $n > 20$. For the $5snp(^1P_1)$ states, we use data from [33], which include experimental energies for $21 \leq n \leq 33$, and calculated energies for $34 \leq n \leq 60$, which do not come with experimental uncertainties. Finally, for the $5snd(^1D_2)$ states, we use experimental data from [33] and [34] for the ranges $21 \leq n \leq 51$ and $52 \leq n \leq 70$ respectively.

B. Model Potential

While computing the one-electron reduced matrix elements of the dipole operator, we use the three-parameter model potential of Ref. [35] describing interaction of the Ry electron with the residual atomic core,

$$U_l(r) = Be^{-Cr} - \frac{1 + (Z-1)e^{-Ar}}{r} + \frac{l(l+1)}{2r^2}. \quad (13)$$

In Ref. [35] the parameters (A, B, C) of this model potential were obtained by fitting its eigenspectrum to experimental data [33, 34] to minimize the differences between numerical and experimental energies for various terms such as 1S_0 , 1P_1 , 1D_2 . Because we need accurate energy denominators in (7) and (9), we fit the energy denominators from the model potential to the experimental energy denominators, rather than fitting the energies from the model potential to experimental energies. The potential quoted in Ref. [35] yields differences between the numerical and experimental energies that are comparable to the experimental energy denominators. Therefore we have modified some of the parameters in [35] to match the experimental energy denominators at high- n ($n \gtrsim 30$); the revised set of parameters is listed in Table I. The parameters marked with asterisks are those that are modified from the ones tabulated in Ref. [35].

The effects of perturbers on the $5sns(^1S_0)$, $5snp(^1P_1)$ and $5snd(^1D_2)$ series are analyzed based on a Multi-channel Quantum Defect Theory (MQDT) approach in Ref. [26] which reports channel fractions in these series. For example, in the $5sns(^1S_0)$ series, the main perturbing channels are $4dnd(^1S_0)$ and $4dnd(^3P_0^e)$ and they account for much less than a percent in the character of the $5sns(^1S_0)$ states for $n > 8$. In the $5snp(^1P_1)$ series, $4dnp(^1P_1)$ accounts for less than 5% for $n > 10$. Finally, in the $5snd(^1D_2)$ series, $4dns(^1D_2)$ have channel fractions below 4% for $n > 10$, in addition to $5pnp$ which accounts for much less than a percent. Mixing from the triplet character through the $4dns(^3D_2)$ is also below one

percent except for $n = 15$ and 16 after which its channel fraction drops to well below a percent. Of particular interest to us in our Fig. 4 is $n = 18$: mixing from the $4d18s(^1D_2)$ is 2% whereas all the other perturbers contribute less than one percent.

To take the perturbed nature of the Ry series into account, we evaluate the C_6 coefficients using experimental energies in the denominator of Eq. (7) and (8). However, the energy spectrum of the model potential (13) is smooth, and it cannot reproduce the perturbed energy levels. Therefore it cannot reflect the effect of the perturbers on the radial matrix elements. The model potential (13) is similar to the one in Ref. [35, 36] where the authors compare calculations of C_6 coefficients using the Coulomb approximation [37] and a model potential like the one we use in our calculations. They conclude that the radial matrix elements obtained using this model potential and the Coulomb approximation typically differ by about ~ 0.1 a.u., and that this translates to about 0.5% difference between the C_6 coefficients for $n \sim 20$.

Furthermore, comparison with experimental Stark maps of Ry states has shown that treating a Ry state of an alkaline-earth metal in the single-electron model to calculate the dipole matrix elements [38] yields satisfactory results for $n < 20$, specifically down to $n = 12$ for Sr. Subsequently, the single-active electron approach for the calculation of the dipole matrix elements seems adequate for our goals.

The radial wave functions in the Coulomb approximation are obtained for hydrogen using the correct experimental energies and integrating the radial Schrödinger equation [38]. This gives the correct energy and the large- r behavior, but incorrect behavior near the core. For the dipole matrix elements, the correct energy and the asymptotic behavior are important. In case the error introduced by the Coulomb approximation in Ref. [36] dominates the total error, in Appendix B, we estimate how large the errors in our calculated matrix elements need to be to increase the sizes of the error bars to effectively recover the n^{11} non-monotonic scaling.

In Appendix B, we first express the error in our dipole matrix elements as an uncertainty $\delta(\nu_n)$ in the quantum defects $\nu_n = n - n^*$. We then show that $\delta(\nu_n)$ must be significantly larger than the variation of the quantum defects across the 1P_1 and 1D_2 Ry series reported in [36] if the error bars are to become large enough to include the monotonic behavior. Furthermore, $\delta(\nu_n)$ must be also significantly larger than the difference between the calculated quantum defects using the model potential (13) and the quantum defects from experimental data.

IV. RESULTS

Because the numerator of δE_{vdW} is proportional to the fourth power of the dipole operator ($\propto n^8$) and the energy

TABLE I: Parameters A, B , and C of the model potential (13) for the Rydberg electron in the $5sns(^1S_0)$, $5snp(^1P_1)$ and $5snd(^1D_2)$ states of strontium. Most of the parameters are from Ref. [35], except the ones marked with asterisks, which were determined in this work by minimizing the differences between the experimental and the numerical values of energy denominators in the second order $^1S_0 + ^1S_0$ (top) and $^1P_1 + ^1P_1$ (bottom) van der Waals interactions.

	$5sns(^1S_0) + 5sns(^1S_0)$		
	A	B	C
1S_0	3.762	-6.33	1.07
1P_1	2.84*	-1.86	1.10
1D_2	2.78	-9.06	2.31
	$5snp(^1P_1) + 5snp(^1P_1)$		
	A	B	C
1S_0	5.599*	-6.33	1.07
1P_1	3.49	-1.86	1.10
1D_2	2.588*	-9.06	2.31

denominator scales as $1/n^3$ for large n , the C_6 coefficient is expected to scale as n^{11} . Although this behavior is exact for hydrogen, non-hydrogenic systems deviate from this scaling law: the softer the atomic core the more deviation from the n^{11} scaling law there is. Below we report C_6 coefficients scaled by n^{11} , $\tilde{C}_6 = C_6/n^{11}$. Therefore, any residual n -dependence leftover in \tilde{C}_6 is atom and state dependent. After scaling by n^{11} , there are two kinds of residual n -dependence left: (1) monotonic dependence on n , which stems from the Ry electron polarizing the atomic core, and (2) any resonance-like behavior such as the series interaction between the Ry series. The latter is the focus of our paper.

The scaled $\tilde{C}_6 = C_6/n^{11}$ coefficients for the van der Waals interaction between pairs of $5sns(^1S_0)$ and $5snp(^1P_{1,x})$ atoms are plotted as a function of n in Figs. 3 and 4. We choose to scale by n^{11} rather than $(n^*)^{11}$ because this gives us a smaller slope for the residual monotonic n -dependence in Figs. 3 and 4 since $n > n^*$.

A. C_6 for the $5sns(^1S_0)$ states

In Fig. 3, open blue diamonds show the \tilde{C}_6 coefficients calculated using Eq. (7) in which both the energy denominator and the one-electron orbitals in the reduced matrix elements are calculated using the model potential (13). The parameters in this model potential are adjusted from those listed in Ref. [35] to match the experimental energy denominators. This curve matches the data reported in Ref. [36] well (open red circles) for all n quoted in [36]. However, around $n \approx 12$, the \tilde{C}_6 coef-

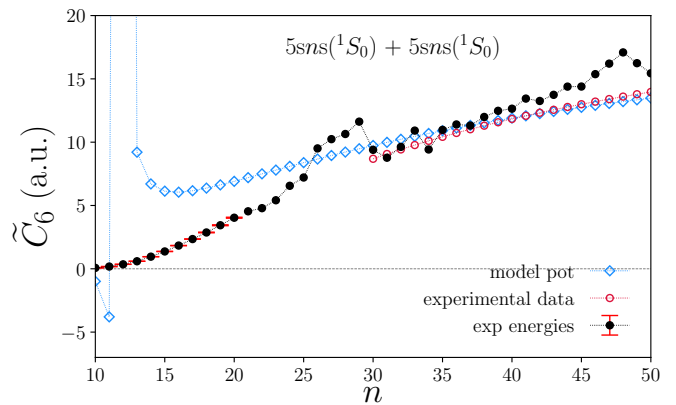


FIG. 3: (Color online) Residual n -dependence of the C_6 coefficients ($\tilde{C}_6 = C_6/n^{11}$) for the $5sns(^1S_0) + 5sns(^1S_0)$ van der Waals interaction in Sr. The blue open diamonds are calculated using the model potential quoted in the text. These match the experimental data from Ref. [36] (red open circles) in the high- n region. Replacing numerical energies from the model potential in the energy denominator with experimental energies results in solid black points. Positive values of \tilde{C}_6 coefficients imply attractive vdW interactions. Error bars are calculated for $n < 20$, beyond which no experimental uncertainties are reported.

n	\tilde{C}_6	$\delta\tilde{C}_6$	$ \delta\tilde{C}_6/\tilde{C}_6 $
10	-0.015	0.0002	0.0125
12	6.72	1.41	0.21
14	-0.12	0.008	0.07
16	3.22	0.13	0.04
18	-37.28	16.35	0.44
20	-1.72	0.017	0.01

TABLE II: Tabulated values of the \tilde{C}_6 coefficients for the $5snp(^1P_{1,x}) + 5snp(^1P_{1,x})$ interaction (Fig. 4), the propagated uncertainties from the energy denominators $\delta\tilde{C}_6$, and the corresponding fractional uncertainties $|\delta\tilde{C}_6/\tilde{C}_6|$ in the range of n for which there is uncertainty data in [32].

icients become extremely large due to almost vanishing energy denominator. Keeping in mind that the energies used in generating this set of \tilde{C}_6 were calculated from the model potential (13), we find that the fitted potential has the pathological behavior at these low- n such that the energy denominator flips sign going from $n = 12$ to 11. This results in an unphysical peak at $n = 12$. A side effect of this is the overestimation of the \tilde{C}_6 coefficients for n up to around 25 due to the large contribution from $n = 12$ intermediate state to the \tilde{C}_6 coefficients of the nearby states.

On the other hand, replacing the numerically calculated energies in the denominator of (7) by experimental values [32–34] results in the solid black points. While

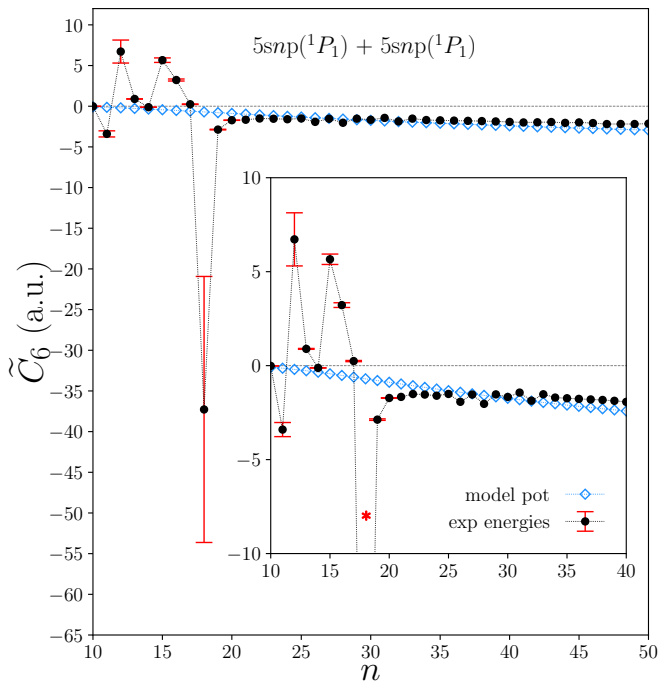


FIG. 4: (Color online) Similar to Fig. 3 but for the $5snp(^1P_{1,1_x}) + 5snp(^1P_{1,1_x})$ interaction. The blue open diamonds are evaluated using matrix elements and energies obtained from the model potential and solid black points using experimental energies in the energy denominator. The red star denotes the data point for $n = 18$ outside the plot range: $\tilde{C}_6(n = 18) \simeq -37$ a.u. The large error bar at $n = 18$, like the large deviation in the \tilde{C}_6 value, stems from near degeneracy in the energy denominator.

matching the other two sets of data well at high n , these keep monotonically decreasing for n below 20 due to the existence of a soft core. We display error bars indicating the propagated uncertainties in the calculated \tilde{C}_6 coefficients in the range $n \leq 20$ where reported experimental data in Ref. [32] also includes the uncertainties. Although these error estimates do not account for errors in the matrix elements incurred using a model potential as discussed in III B, they show that the uncertainties which stem from the energy denominators are very small.

B. C_6 for the $5snp(^1P_{1,1_x})$ states

Unlike the $5sns(^1S_0) + 5sns(^1S_0)$ interaction, numerically calculated values of \tilde{C}_6 using the model potential (13) between $5snp(^1P_{1,1_x})$ states do not display the same pathological behavior at low n (open blue diamonds in Fig. 4). Replacing the numerically calculated energies in the denominators of Eq. (8) with experimental ones listed in [32–34] changes the \tilde{C}_6 coefficients very little for $n \gtrsim 20$ (solid black points).

We observe an unusual feature in the low- n region below $n = 20$: the \tilde{C}_6 coefficients display a non-monotonic behavior. Unlike the unphysical peak at $n = 12$ in the $^1S_0 + ^1S_0$ interaction (Fig. 3), which stems from inaccurate representation of the soft-core potential at small distances, the non-monotonic features in the $^1P_{1,1_x} + ^1P_{1,1_x}$ are real: they are etched in energy denominators derived from experimental spectra. For example, in the interaction between two $5s18p(^1P_{1,1_x})$ states, the energy denominator in Eq. (8) involving the $5s18p(^1P_{1,1_x})$, $5s16d(^1D_2)$ and $5s18d(^1D_2)$ states becomes unusually small, which gives the large peak at $n = 18$. The behavior of the energy denominator in the $nP + nP \rightarrow n'D + n''D$ channel can be seen in Fig. 5. In order to emphasize its non-monotonic nature, we have plotted the scaled energy denominator $1/(n^{*3}\Delta E)$ rather than ΔE . Here ΔE is the energy difference $2E_{nP} - (E_{n'D} + E_{n''D})$, and $n^* = n - \nu_n$ is the effective principal quantum number where the quantum defect ν_n is calculated using the Rydberg-Ritz formula

$$\nu_n = \nu_n^{(0)} + \frac{\nu_n^{(2)}}{(n - \nu_n^{(0)})^2} + \frac{\nu_n^{(4)}}{(n - \nu_n^{(0)})^4}. \quad (14)$$

Here the coefficients $\nu_n^{(0)}$, $\nu_n^{(2)}$, and $\nu_n^{(4)}$ are obtained from fitting to experimental data in the range $10 \leq n \leq 29$ for the $5snp(^1P_1)$ series, and $20 \leq n \leq 50$ for the $5snd(^1D_2)$ series (Table 2 in [36]).

Notice that the energy denominators associated with the channels $nP + nP \rightarrow (n-1)D + (n-1)D$ and $nP + nP \rightarrow nD + nD$ are well behaved for all n (open green diamonds and open blue squares). This is to be expected from a hydrogen-like spectrum where the nearest-neighbor energy spacing scales as $1/n^3$ for all n . On the other hand, whereas $1/(n^{*3}\Delta E)$ is flat above $n \sim 20$, it is far from regular below $n \sim 20$ in the $nP + nP \rightarrow nD + (n-1)D$ channel. Particularly at $n = 18$, the energy difference $2E_{nP} - (E_{nD} + E_{(n-1)D})$ is unusually small resulting in the large peak in \tilde{C}_6 . Besides being flat above $n \sim 20$, $1/(n^{*3}\Delta E)$ is also much smaller than the values at the peaks below $n \sim 20$, which translates into large \tilde{C}_6 coefficients for the van der Waals interactions between the $^1P_{1,1_x}$ states in the region $n \lesssim 20$. The error bars in Figs. 4 and 5 show that taking the experimental uncertainties into account does not change the qualitative picture for $n < 20$. It is also worth reiterating that the open data points for \tilde{C}_6 in Fig. 4 obtained using experimental energies but do not include configuration interaction for the matrix elements.

The deviation of the nearest-neighbor energy differences from the hydrogenic $1/n^{*3}$ scaling is a consequence of the series perturbation. The energies of the $5sns(^1S_0)$ states almost perfectly scale as $1/n^{*2}$ for all n^* , whereas $5snp(^1P_1)$ and $5snd(^1D_2)$ states increasingly deviate from this scaling as n^* gets below ~ 20 . This is because the states with higher angular momenta are more likely to be perturbed by other series. For a Rydberg series to be perturbed by another state, the energy

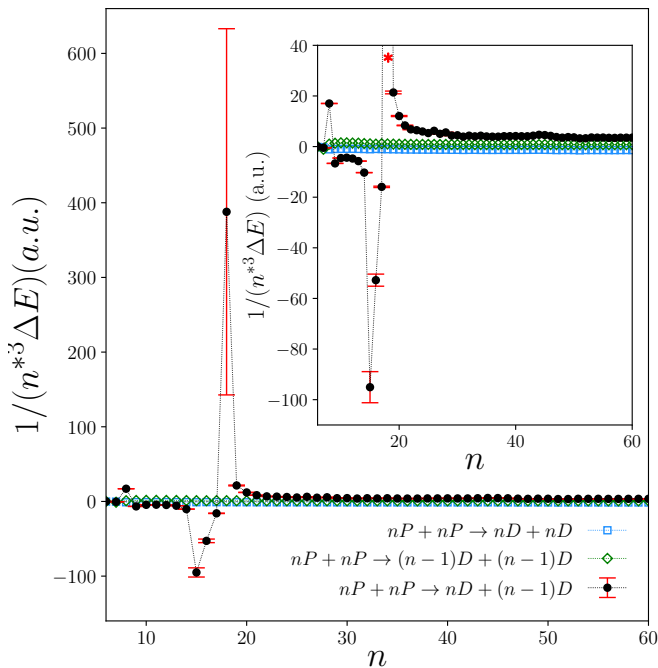


FIG. 5: (Color online) The scaled energy denominator in the second order perturbation theory expression for the \tilde{C}_6 coefficients in the long range interaction between two $5snp(^1P_{1,x})$ Sr atoms. ΔE scales as $1/n^3$ as expected for the $nP + nP \rightarrow (n-1)D + (n-1)D$ and $nP + nP \rightarrow nD + nD$ interaction channels over the entire n -range. For the $nP + nP \rightarrow nD + (n-1)D$ channel, however, this scaling breaks down for $n \lesssim 20$ and $1/(n^3 \Delta E)$ attain large values and changes sign. This “resonance-like” structure is facilitated by an unusually small ΔE around $n \sim 17$ and is possible because of the highly perturbed nature of the $5snd(^1D_2)$ series in Sr. The error bars for the $nP + nP \rightarrow nD + (n-1)D$ channel show that taking the experimental uncertainties into account does not change the qualitative picture for $n < 20$.

of the perturber state needs to be below the ionization threshold for the Rydberg series. Furthermore, it needs to have the same J and the parity for the associated Coulomb integral to be non-zero. Researching the literature, we have found that the $5snd(^1D_2)$ series of Sr is perturbed by the $4d^2(^1D_2^e)$, $5p_{3/2}^2(^1D_2^e)$ and $4d6s(^1D_2^e)$ states, all of which lie below the ionization threshold of the $5snd(^1D_2^e)$ series at $45,932 \text{ cm}^{-1}$ [26]. Other candidates with higher angular momenta that could perturb the $5snd(^1D_2^e)$ series are $4dng(^1D_2^e)$, however, we could not find experimental data to confirm that these states actually lay below $45,932 \text{ cm}^{-1}$. We find that the $4d6s(^1D_2^e)$ state perturbs states with $n = 11 - 17$, $5p^2(^1D_2^e)$ perturbs states with $n = 5 - 6$ and $4d^2(^1D_2^e)$ state perturbs the state with $n = 12$ in the $5snd(^1D_2^e)$ series. A detailed analysis of the $5sns(^1S_0)$, $5snp(^1P_1)$ and $5snd(^1D_2)$ series and their perturbers is given in [26]. In contrast with the $5snp(^1P_{1,x}) + 5snp(^1P_{1,x})$ interac-

tion, we see no contribution from perturber states for the $5sns(^1S_0) + 5sns(^1S_0)$ interaction at low- n due to lower angular momentum of the perturber states in the 1S_0 series [26].

Furthermore, the sum in Eq. (4) is essentially dominated by one term with the smallest energy denominator. The energy denominator of this term determines the sign of the \tilde{C}_6 coefficient. The numerator is positive and, therefore, does not change the sign of the dominant term. The result is that the sign changes seen in the \tilde{C}_6 coefficients in Fig. 4 cannot be undone by changing the values of the dipole matrix elements. Therefore, the non-monotonic behavior seen in Fig. 4 stems from the energy denominator and would not disappear if more accurate radial matrix elements were used in our calculations.

C. Fitting \tilde{C}_6 to rational functions of n

Keeping in mind practical applications, we fitted the \tilde{C}_6 coefficients to rational functions of n . It is a common practice to fit these data to second or third degree polynomials [36]. One problem with this choice of fitting functions is that they can display wildly different behavior outside the fitted range of n and they diverge as $n \rightarrow \infty$. To mitigate this problem, we fit our data to *rational* functions which approach a fixed value as $n \rightarrow \infty$. In particular, we choose $(an + b)/(n + d)$ and $(an^2 + bn + c)/(n^2 + en + f)$ where a, b, c, d, e and f are fitting parameters. These parameters are listed in Table III. In the high- n limit, both these functions approach a . Notice that these are smooth functions and cannot reproduce the non-monotonic behavior seen in Fig. 4. Results of our least-squares fit for the \tilde{C}_3 coefficients are tabulated in Table III. Parameters in Table III indicate in the limit $n \rightarrow \infty$ the van der Waals interactions between pairs of $5sns(^1S_0)$ atoms is roughly a factor of 3 stronger than those between pairs of $5snp(^1P_{1,x})$ atoms. On the other hand, it is clear from Fig. 4 that picking $n = 18$ results in much stronger van der Waals interactions between the $5snp(^1P_{1,x})$ states than what would be expected from the fits quoted in Table III.

V. ANGULAR DEPENDENCE OF THE VAN DER WAALS INTERACTION

Detailed derivation of the angular dependence of van der Waals interaction can be found in the Appendix. The dependence of the \tilde{C}_6 coefficients for the $^1P_{1,x} + ^1P_{1,x}$ van der Waals interaction on the angle θ that the quantizing B-field makes with the internuclear axis can be expressed in term of Legendre polynomials $P_0(\cos\theta)$, $P_2(\cos\theta)$ and $P_4(\cos\theta)$. The angular part of the interaction energy δE_{vdW} (A1) is contained in the square-

TABLE III: Fit parameters for the scaled \tilde{C}_6 for fits of the form $(an + b)/(n + d)$ and $(an^2 + bn + c)/(n^2 + en + f)$ for the $^1S_0 + ^1S_0$ and $^1P_1 + ^1P_1$ van der Waals interactions. The χ^2 parameter for the lower order fit is $\lesssim 0.05$ and $\chi^2 < 10^{-4}$ in the higher order fit. One needs to go to $n = 200$ for the difference between the two fits for the \tilde{C}_6 coefficients to become $\sim 10\%$.

	$(an + b)/(n + d)$		
	a	b	d
$\tilde{C}_6(^1S_0 + ^1S_0)$	27.268	-116.556	41.926
$\tilde{C}_6(^1P_{1,1x} + ^1P_{1,1x})$	-11.036	112.5	97.176

	$(an^2 + bn + c)/(n^2 + en + f)$				
	a	b	c	e	f
$\tilde{C}_6(^1S_0 + ^1S_0)$	22.821	-473.021	3136.018	6.791	-129.797
$\tilde{C}_6(^1P_{1,1x} + ^1P_{1,1x})$	-6.342	97.465	-390.021	22.228	260.072

bracketed terms in Eq. (A4) and can be written as

$$\begin{aligned}
 f_{ss}(\theta) &= \frac{1}{45} + \frac{2}{63}P_2(\cos\theta) + \frac{2}{35}P_4(\cos\theta), \\
 f_{dd}(\theta) &= \frac{271}{4500} + \frac{32}{1575}P_2(\cos\theta) + \frac{1}{1750}P_4(\cos\theta), \\
 f_{sd}(\theta) &= \frac{23}{225} - \frac{1}{630}P_2(\cos\theta) + \frac{1}{175}P_4(\cos\theta),
 \end{aligned}$$

for the three channels involved, where we have denoted the angular part of the vdW interaction energy in Eq. (A4) with the functions f . Finally, we express the C_6 coefficients from (A4) using $\delta E_{\text{vdW}} = -C_6/R^6$:

$$C_6 = f_{ss}(\theta)S_{ss} + f_{dd}(\theta)S_{dd} + f_{sd}(\theta)S_{sd}. \quad (16)$$

Here the reduced sums S_{ss} , S_{dd} and S_{sd} are defined in Eq. (9).

The contributions from these three channels to the angular distribution of the coefficients $|\tilde{C}_6|$ for three n values are plotted in Fig. 6. The $nP + nP \rightarrow n'S + n''S$ channel contribution is depicted by the blue dotted curves, the $nP + nP \rightarrow n'D + n''D$ channel by the red dashed and the $nP + nP \rightarrow n'S + n''D$ channel by the brown dot-dashed curves. The total is plotted as the solid green curve in each case. It is clear from Eqs. (15) and Fig. 6 that the $nP + nP \rightarrow n'S + n''S$ channel is dominated by $P_4(\cos\theta)$ whereas the $nP + nP \rightarrow n'D + n''D$ channel is dominated by $P_2(\cos\theta)$. All three channels contribute comparably to the total \tilde{C}_6 over the range of all angles for $n = 30$ and 50 which are states in the unperturbed part the Rydberg series with \tilde{C}_6 behaving monotonically in Fig. 4. For $n = 18$ however, the total \tilde{C}_6 is entirely determined by the $nP + nP \rightarrow n'D + n''D$ channel. This is because the resonance-like peak at $n = 18$ in Fig. 4 is due to the highly perturbed nature of the $5snd(^1D_2)$ Rydberg series which result in an unusually small energy denominator for $n = 18$ in the $nP + nP \rightarrow n'D + n''D$

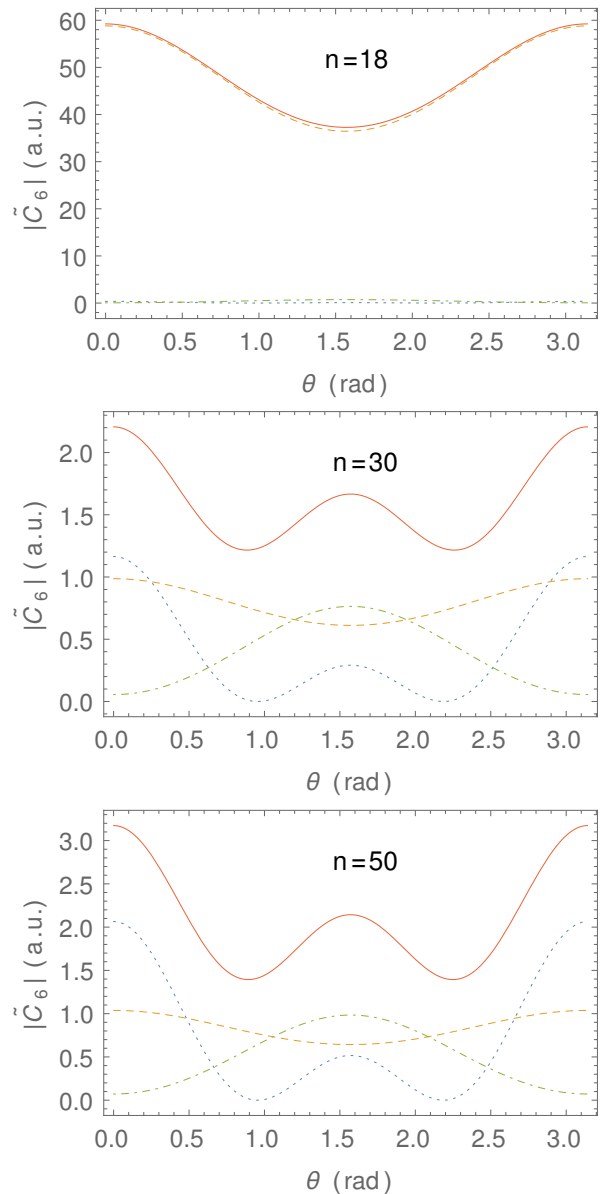


FIG. 6: (Color online) Angular distributions of the $|\tilde{C}_6|$ coefficients for the van der Waals interaction between two $5snp(^1P_{1,1x})$ Sr atoms (solid green curves) for various n , and individual contributions from different intermediate channels: $5sns(^1S_0) + 5sn's(^1S_0)$ (blue dotted), $5snd(^1D_2) + 5sn'd(^1D_2)$ (dashed red), and $5sns(^1S_0) + 5sn'd(^1D_2)$ (dotted dash brown). Note that the $5sns(^1S_0) + 5sn's(^1S_0)$ channel is dominated by $P_4(\cos\theta)$ whereas the $5snd(^1D_2) + 5sn'd(^1D_2)$ channel is dominated by $P_2(\cos\theta)$. It is clear from the top panel that \tilde{C}_6 is entirely determined by the $P_2(\cos\theta)$ character of the $5snd(^1D_2) + 5s(n-1)d(^1D_2)$ channel at $n = 18$, where the $5snd(^1D_2)$ series is strongly perturbed.

channel. The results we quote in Fig. 4 and in Table III are for $\theta = \pi/2$ which corresponds to the middle peak in the solid green curves in Fig. 6.

VI. CONCLUSION

Motivated by the recent interest in using divalent Rydberg atoms in quantum information processing we have calculated the van der Waals coefficients for two interacting Sr Rydberg atoms. We computed the C_6 coefficients for the van der Waals interactions between two $5sns(^1S_0)$ and two $5snp(^1P_{1,M_x=1})$ Sr atoms. We find that our results are in good agreement with previously reported values in Ref. [36], which tabulated these C_6 coefficients for $n \geq 30$. We also find that for $n < 20$, the C_6 and van der Waals coefficients for the $5snp(^1P_1)$ states show strong non-monotonic deviations from the hydrogenic n^{11} scaling due to the highly perturbed nature of the $5snd(^1D_2)$ series as discussed in Ref. [26], which results in small energy denominators in the second-order expressions for the energy shifts. As a result, the C_6 coefficients display highly non-monotonic behavior and change sign in the small n -region suggesting that the interaction can be made attractive or repulsive by choosing appropriate n . Particularly at $n = 18$, \tilde{C}_6 is much larger than it is in any other state for the entire n -range we consider, which

provides a possibility for engineering strongly asymmetric long-range interactions by contrasting it with the van der Waals interaction between two Sr atoms in $5sns(^1S_0)$ states. The error bars in the low n -region obtained by propagating reported experimental uncertainties show that taking the experimental uncertainties into account does not change this picture for $n < 20$.

VII. ACKNOWLEDGEMENTS

This work was supported by the National Science Foundation (NSF) Grant No. PHY-1212482. A.D. was also supported by the Simons foundation as a Simons fellow in theoretical physics, and by NSF Grant No. PHY-2207546. T.T. and A.D. would like to thank the Institute for Theoretical Atomic, Molecular and Optical Physics (ITAMP) and the Harvard University Physics Department for their hospitality, where a part of this work was carried out. The authors would like to thank P. Kómár and M. D. Lukin for valuable discussions.

Appendix A: Derivation of van der Waals expressions

Here we derive an expression for the van der Waals interaction energy correction for a pair of atoms, δE_{vdW} . The sets of quantum numbers of the two atoms (I and II) in the LSJ coupling scheme will be denoted as $\gamma_1[L_1S_1J_1]_{M_1}$ (I) and $\gamma'_1[L'_1S'_1J'_1]_{M'_1}$ (II), where the set of quantum numbers nl are denoted by γ . In particular we are interested in the van der Waals interactions between (1) two $5sns(^1S_0)$ atoms with $M_B = M'_B = 0$, and (2) $5snp(^1P_{1,M})$ and $5snp(^1P_{1,M'})$ atoms with $M_B = M'_B = 1$.

The second order energy shift is given by

$$\delta E_{\text{vdW}}(\gamma_1[L_1S_1J_1]_{M_1}(\text{I})\gamma'_1[L'_1S'_1J'_1]_{M'_1}(\text{II})) = \frac{1}{R^6} \quad (\text{A1})$$

$$\times \sum_{\substack{\gamma_2, \gamma'_2 \\ J_2, J'_2 \\ M_2, M'_2}} \frac{\left| \left\langle \gamma_1[L_1S_1J_1]_{M_1}(\text{I})\gamma'_1[L'_1S'_1J'_1]_{M'_1}(\text{II}) \left| V_{DD} \right| \gamma_2[L_2S_2J_2]_{M_2}(\text{I})\gamma'_2[L'_2S'_2J'_2]_{M'_2}(\text{II}) \right\rangle \right|^2}{(E_{\gamma_1[L_1S_1J_1]} + E_{\gamma'_1[L'_1S'_1J'_1]}) - (E_{\gamma_2[L_2S_2J_2]} + E_{\gamma'_2[L'_2S'_2J'_2]})},$$

where V_{DD} is the rotated dipole-dipole interaction and the summation is over the intermediate states $|\gamma_2[L_2S_2J_2]_{M_2}; \gamma'_2[L'_2S'_2J'_2]_{M'_2}\rangle$. Because we are interested in the van der Waals interaction between atoms in identical electronic configurations, we take $n_1 = n'_1 \equiv n_r$ and $l_1 = l'_1 \equiv l_r$.

To express the two-electron reduced matrix elements in terms of one-electron orbitals, we first transform the matrix element $\langle ^1S_0 || D || ^1P_1 \rangle$ from the LSJ to the LS coupling,

$$\langle \gamma_1[L_1S_1J_1] || D || \gamma_2[L_2S_2J_2] \rangle = (-1)^{L_1+S_2+J_2+1} \sqrt{[J_1][J_2]} \quad (\text{A2})$$

$$\begin{Bmatrix} L_1 & J_1 & S_2 \\ J_2 & L_2 & 1 \end{Bmatrix} \langle \gamma_1 L_1 || D || \gamma_2 L_2 \rangle \delta_{S_1, S_2}.$$

In the independent-particle approximation, the two-electron matrix element can be expressed in terms of a reduced matrix element involving only the single electron orbitals (see Ref. [39] for details). Since we are only interested in the singlet states $S_1 = S_2 = 0$ and we obtain

$$\langle 5sn\ell(L_1) || D || 5sn'\ell'(L_2) \rangle = \sqrt{[L_1][L_2]} (-1)^{\ell'+L_1+1} \begin{Bmatrix} 1 & L_2 & L_1 \\ 0 & \ell & \ell' \end{Bmatrix} \langle n\ell || d || n'\ell' \rangle. \quad (\text{A3})$$

Here d is the one-particle dipole operator and $D = \sum_{k=1}^2 d_k$ where the sum goes over the two atomic valence electrons. We also assume that the overlap between the $n\ell$ state of the Rydberg electron and the $5s$ state of the valence electron is negligible, which allows us to drop a second term involving $\langle 5s||d||n'\ell' \rangle$ on the right hand side of Eq. (A3). Since Eq. (A3) now involves only the reduced matrix element for the Rydberg electron, we have removed the summation over the valence electrons and dropped the subscript in d_k . Finally, we obtain

$$\begin{aligned} \delta E_{\text{vdW}}([L_1 S_1 J_1]_{M_1}(\text{I}) [L'_1 S'_1 J'_1]_{M'_1}(\text{II})) &= \frac{1}{R^6} \sum_{\substack{l_2, l'_2 \\ J_2, J'_2}} \\ &\left[\sum_{\substack{M_1, M'_1 \\ M_2, M'_2}} \sigma_\theta(J_1, J'_1, M_1, M'_1; J_2, J'_2, M_2, M'_2) \sigma_\theta(J_2, J'_2, M_2, M'_2; J_1, J'_1, M_1, M'_1) \right] \\ &\times \left[A(L_1, S_1, J_1, \ell_1; L_2, S_2, J_2, \ell_2) A(L'_2, S'_2, J'_2, \ell'_2; L'_1, S'_1, J'_1, \ell'_1) \right]^2 \\ &\times \sum_{n_2, n'_2} \frac{|\langle n_r l_r || d || n \ell_2 \rangle|^2 |\langle n_r l_r || d || n' \ell'_2 \rangle|^2}{(E_{L_1 S_1 J_1} + E_{L'_1 S'_1 J'_1}) - (E_{L_2 S_2 J_2} + E_{L'_2 S'_2 J'_2})}. \end{aligned} \quad (\text{A4})$$

Here we have factored out the summation over the magnetic quantum numbers which depends on the rotation angle of the quantization axis. The function σ_θ describes the rotation of the quantization axis with respect to the inter-atomic axis, and the function A involves the factors from breaking up the two-electron reduced matrix elements into reduced one-electron matrix elements in the LS coupling scheme. Explicitly, these functions are given by

$$\begin{aligned} \sigma_\theta(J_1, J'_1, M_1, M'_1; J_2, J'_2, M_2, M'_2) &= \sum_{\mu} w_{\mu}^{(1)}(-1)^{M_1+M'_1} d_{M_1-M_2, \mu}^{(1)}(\theta) d_{M'_2-M'_1, -\mu}^{(1)}(\theta) \\ &\times \begin{pmatrix} J_1 & 1 & J_2 \\ -M_1 & M_1 - M_2 & M_2 \end{pmatrix} \begin{pmatrix} J'_1 & 1 & J'_2 \\ -M'_1 & -(M'_2 - M'_1) & M'_2 \end{pmatrix} \\ A(L_1, S_1, J_1, l_1; L_2, S_2, J_2, l_2) &= (-1)^{L_1+S_2+J_2+l_2+J_1} \sqrt{[J_1][L_1][J_2][L_2]} \\ &\times \begin{Bmatrix} 1 & J_2 & J_1 \\ 0 & l_1 & l_2 \end{Bmatrix} \begin{Bmatrix} L_1 & J_1 & S_2 \\ J_2 & L_2 & 1 \end{Bmatrix}, \end{aligned} \quad (\text{A5})$$

where $[J] = (2J + 1)$ and $d_{M, \mu}^{(1)}(\theta)$ are Wigner functions. The angular dependence in Eq. (A4) can be expressed as a linear combination of Legendre polynomials $P_0(\cos \theta)$, $P_2(\cos \theta)$ and $P_4(\cos \theta)$. Finally, the C_6 coefficients can be extracted from this expression according to $\delta E_{\text{vdW}} = -C_6/R^6$.

For the vdW interaction between two atoms in the $5snp(^1P_{1,1_x})$ states, the general expression (A4) can be broken into contributions from three channels: (1) $nP + nP \rightarrow n'S + n''S$, (2) $nP + nP \rightarrow n'D + n''D$ and (3) $nP + nP \rightarrow n'S + n''D$. Denoting the angular factors inside the closed brackets in Eq. (A4) with functions $f_{ss}(\theta)$, $f_{dd}(\theta)$ and $f_{sd}(\theta)$, we can express (A4) as

$$\delta E_{\text{vdW}} = -\frac{1}{R^6} \left(f_{ss}(\theta) S_{ss} + f_{dd}(\theta) S_{dd} + f_{sd}(\theta) S_{sd} \right), \quad (\text{A6})$$

where the reduced sums S_{ss} , S_{ss} and S_{ss} are defined in Eq. (9).

Appendix B: Error estimates for the dipole matrix elements

Here we show how big the errors in our calculated matrix elements need to be to increase the sizes of the error bars in Fig. 4, effectively recovering the n^{11} non-monotonic scaling (blue diamonds in Fig. 4). Specifically, we conclude that to change the size of the error bar for

$n = 18$ so that it becomes large enough to encapsulate its monotonically scaling counterpart (blue diamond at $n = 18$), the error in the corresponding radial matrix element needs to be much larger than what is reported in [36]. Therefore, we conclude that using the model potential does not alter our qualitative arguments.

In Sec. III A, we estimated the uncertainty in the C_6 coefficients under the assumption that the uncertainty in

the dipole matrix elements were zero, *i.e.*, $\delta(V_{j,k}) = 0$ (Eq. (10)). Instead, we now start with the fractional errors [40]. Based on Fig. 5, we will assume that the sum (4) is dominated by a single term, $nP + nP \rightarrow nD + (n-1)D$ where $n = 18$. In the single-electron, single-term approximation, there are two distinct matrix elements in $V_{j,k}$, which we label $d_{n_r,n}$ and $d_{n_r,n'}$, and we remove the sum. These matrix elements are then squared in the numerator of (4). Therefore, the fractional error is

$$\left(\frac{\delta C_6}{C_6}\right)^2 = 2 \left[\left(\frac{\delta d_{n_r,n}}{d_{n_r,n}}\right)^2 + \left(\frac{\delta d_{n_r,n'}}{d_{n_r,n'}}\right)^2 \right] + \left(\frac{\delta \Delta E}{\Delta E}\right)^2. \quad (\text{B1})$$

Here we added the fractional uncertainties in quadrature because the uncertainties in the energies and the dipole matrix elements are independent. In estimating the uncertainties in Sec. III A, we assumed that $\delta d_{n_r,n} = \delta d_{n_r,n'} = 0$. This assumption leads to

$$\frac{\delta C_6^{(0)}}{C_6^{(0)}} := \frac{\delta C_6}{C_6} = \frac{\delta \Delta E}{\Delta E}. \quad (\text{B2})$$

From Table II, $\delta C_6^{(0)}/C_6^{(0)} = 0.44$. When $n = n_r = 18$ and $n' = 17$, the matrix elements d_{n_r,n_r} and d_{n_r,n_r-1} scale as n_r^2 with similar coefficients [41] which cancel from the fractional errors, and $\delta d_{n_r,n_r}/d_{n_r,n_r} \approx \delta d_{n_r,n_r-1}/d_{n_r,n_r-1}$. This allows us to write from (B1)

$$\left(\frac{\delta d_{n_r,n_r}}{d_{n_r,n_r}}\right)^2 = \frac{1}{4} \left[\left(\frac{\delta C_6^{(1)}}{C_6^{(1)}}\right)^2 - \left(\frac{\delta C_6^{(0)}}{C_6^{(0)}}\right)^2 \right], \quad (\text{B3})$$

where $C_6^{(1)}$ is the actual value of the C_6 coefficient that takes the uncertainties in the dipole matrix elements into account. For the error bars in Fig. 4 to become large enough to encapsulate the C_6 coefficients obtained using the model potential alone (blue diamonds), $\delta C_6^{(1)}/C_6^{(1)} \approx$

0.98, and $\delta d_{18,18}/d_{18,18} \approx \delta d_{18,17}/d_{18,17} \approx 0.44$. Furthermore, since $d_{n_r,n} \propto (n_r^*)^2 = (n_r - \nu_{n_r})^2$, and the quantum defects ν_{n_r} change little as a function of n [41], we have

$$\frac{\delta d_{n_r,n_r}}{d_{n_r,n_r}} = \frac{2\delta\nu_{n_r}}{(n_r - \nu_{n_r})} \approx 0.44. \quad (\text{B4})$$

For $n_r = 18$, therefore $\delta(\nu_{n_r}) \approx 3.35$. This value can then be regarded as the uncertainty in the quantum defect the $n_r = 18$ states need to have for the corresponding dipole matrix element to become large enough to undo the non-monotonic resonance-like behavior we discuss in this work.

The value $\delta(\nu_n) \approx 3.35$ is, however, too large even for a model potential. For comparison, the quantum defect ν_n varies by 0.55 across the 1S_0 and 1P_1 Ry series, and by 0.34 between the 1P_1 and 1D_2 series of Sr in the n -range of interest. Similarly, across the triplet Ry series, ν_n varies by 0.47 between the 3S_1 and the $^3P_{0,1,2}$ series, and by 0.3 between the $^3P_{0,1,2}$ and $^3D_{1,2,3}$. Even across different species, for example between Sr and Ca, ν_n varies by 0.8 across the $5snp(^1P_1)$ and $4snp(^1P_1)$.

This suggests that $\delta(\nu_{18}) \approx 3.35$ is too large an error to expect in the quantum defect. Therefore, we expect that using a model potential for evaluating the radial wave functions, and the dipole matrix elements is justified in our calculations. For example, the quantum defect for the $5s18p(^1P_1)$ state obtained in [36] by fitting to the Rydberg-Ritz formula (14) using experimental data is 2.71. On the other hand, our model potential yields a quantum defect of 2.33. The difference is chiefly due to two factors: (1) the model potential in [35] fits to experimental energies for $n > 20$ where the quantum defects vary smoothly, and (2) our fit targets the energy denominators rather than the energies as in [36]. Even then the difference is ~ 0.38 , which is well below $\delta(\nu_{18}) \approx 3.35$ necessary to increase the size of the error bar for $n = 18$ in Fig. 4 to include the monotonic behavior.

-
- [1] E. Urban, T. A. Johnson, T. Henage, L. Isenhower, D. D. Yavuz, T. G. Walker, and M. Saffman. Nat. Phys. **5**, 110 (2009)
- [2] A. Gaëtan, Y. Miroshnychenko, T. Wilk, A. Chotia, M. Viteau, D. Comparat, P. Pillet, A. Browaeys, and P. Grangier. Nat. Phys. **5**, 115 (2009)
- [3] I. I. Beterov, M. Saffman, E. A. Yakshina, V. P. Zhukov, D. B. Tretyakov, V. M. Entin, I. I. Ryabtsev, C. W. Mansell, C. MacCormick, S. Bergamini, and M. P. Fedoruk. Physical Review A **88**, 010303 (2013)
- [4] M. Saffman, T. Walker, and K. Mølmer. Rev. Mod. Phys. **82**, 2313 (2010)
- [5] D. Jaksch, J. Cirac, P. Zoller, S. Rolston, R. Côté, and M. Lukin. Phys. Rev. Lett. **85**, 2208 (2000)
- [6] M. Müller, I. Lesanovsky, H. Weimer, H. P. Büchler, and P. Zoller. Phys. Rev. Lett. **102**, 170502 (2009)
- [7] H. Weimer, M. Müller, I. Lesanovsky, P. Zoller, and H. P. Büchler. Phys. Rev. Lett. **6**, 382 (2010)
- [8] T. Pohl, E. Demler, and M. D. Lukin. Phys. Rev. Lett. **104**, 043002 (2010)
- [9] F. Cinti, P. Jain, M. Boninsegni, A. Micheli, P. Zoller, and G. Pupillo. Phys. Rev. Lett. **105**, 135301 (2010)
- [10] M. Saffman and K. Mølmer. Physical Review Letters **102**, 240502 (2009)
- [11] T. Peyronel, O. Firstenberg, Q.-Y. Liang, S. Hofferberth, A. V. Gorshkov, T. Pohl, M. D. Lukin, and V. Vuletić. Nature **488**, 57 (2012)
- [12] D. E. Chang, V. Vuletić, and M. D. Lukin. Nature Photonics **8**, 685 (2014)
- [13] M. Saffman and K. Mølmer. Physical Review A **78**, 012336 (2008)
- [14] F. Robicheaux, D. W. Booth, and M. Saffman. Physical Review A **97** (2018). 1711.10518
- [15] A. Trautmann, M. J. Mark, P. Ilzhöfer, H. Edri, A. El

- Arrach, J. G. Maloberti, C. H. Greene, F. Robicheaux, and F. Ferlaino. *Physical Review Research* **3** (2021). 2105.00738
- [16] R. Mukherjee, J. Millen, R. Nath, M. P. A. Jones, and T. Pohl. *Journal of Physics B: Atomic, Molecular and Optical Physics* **44**, 184010 (2011)
- [17] T. Topcu and A. Derevianko. *Phys. Rev. A* **89**, 023411 (2014)
- [18] X. Xu, T. H. Loftus, J. L. Hall, A. Gallagher, and Y. J. J. *Opt. Soc. Am. B* **20**, 968 (2003)
- [19] U. D. Rapol, A. Krishna, A. Wasan, and N. V. Eur. *Phys. J. D* **29**, 409 (2004)
- [20] B. Hemmerling, G. K. Drayna, E. Chae, A. Ravi, and D. J. M. *New J. Phys.* **16**, 063070 (2014)
- [21] F. Sorrentino, G. Ferrari, N. Poli, R. Drullinger, and T. G. M. *Mod. Phys. Lett.* **20**, 1287 (2006)
- [22] A. Jenkins, J. W. Lis, A. Senoo, W. F. McGrew, and A. M. Kaufman. *Phys. Rev. X* **12**, 021027 (2022)
- [23] S. Ma, A. P. Burgers, G. Liu, J. Wilson, B. Zhang, and J. D. Thompson. *Phys. Rev. X* **12**, 021028 (2022)
- [24] T. F. Gallagher. *Rydberg Atoms* Cambridge Monographs on Atomic, Molecular and Chemical Physics (1994)
- [25] A. Derevianko and H. Katori. *Rev. Mod. Phys.* **83**, 331 (2011)
- [26] C. L. Vaillant, M. P. A. Jones, and R. M. Potvliege. *Journal of Physics B: Atomic, Molecular and Optical Physics* **47**, 155001 (2014)
- [27] F. Robicheaux. *Journal of Physics B: Atomic, Molecular and Optical Physics* **52** (2019)
- [28] B. J. Bloom, T. L. Nicholson, J. R. Williams, S. L. Campbell, M. Bishof, X. Zhang, W. Zhang, S. L. Bromley, and J. Ye. *Nature* **506**, 71 (2014)
- [29] N. Hinkley, J. a. Sherman, N. B. Phillips, M. Schioppo, N. D. Lemke, K. Beloy, M. Pizzocaro, C. W. Oates, and a. D. Ludlow. *Science (New York, N.Y.)* **341**, 1215 (2013)
- [30] A. D. Ludlow, M. M. Boyd, J. Je, E. Peik, and P. Schmidt. *arXiv:1407.3493v1* 1–90 (2014)
- [31] V. K. K. D. A. Varshalovich, A. N. Moskalev. *World Scientific*, 1989 (1989)
- [32] J. E. Sansonetti and G. Nave. *Journal of Physical and Chemical Reference Data* **39**, 033103 (2010)
- [33] P. Esherick. *Physical Review A* **15** (1977)
- [34] D. F. Beigang, R., K. Lucke, A. Timmerman, P.J. West. *Optics Communications* **42**, 19 (1982)
- [35] J. Millen. Durham University (PhD Thesis) **PhD Thesis**, <http://etheses.dur.ac.uk/849/> (2011)
- [36] C. L. Vaillant, M. P. A. Jones, and R. M. Potvliege. *Journal of Physics B: Atomic, Molecular and Optical Physics* **45**, 135004 (2012)
- [37] S. Weber, C. Tresp, H. Menke, A. Urvoy, O. Firstenberg, H. P. Büchler, and S. Hofferberth. *Journal of Physics B: Atomic, Molecular and Optical Physics* **50** (2017)
- [38] M. C. Zhi, C. J. Dai, and S. B. Li. *Chinese Physics* **10**, 929 (2001)
- [39] W. R. Johnson, D. R. Plante, and J. Sapirstein. *Advances In Atomic, Molecular, and Optical Physics* **35**, 255 (1995)
- [40] J. R. J. R. Taylor. *An introduction to error analysis : the study of uncertainties in physical measurements*. University Science Books, Sausalito, California SE - xvii, 327 pages : illustrations ; 26 cm, second edi edition (1997)
- [41] J. H. Hoogenraad and L. D. Noordam. *Physical Review A - Atomic, Molecular, and Optical Physics* **57**, 4533 (1998)